

# Receiver-pair seismic interferometry applied to body-wave USArray data

Elmer Ruigrok\*

*Department of Geoscience and Engineering, Delft University of Technology, Stevinweg 1, 2628 CN Delft, the Netherlands. E-mail: [e.n.ruigrok@tudelft.nl](mailto:e.n.ruigrok@tudelft.nl)*

Accepted 2014 May 6. Received 2014 March 21; in original form 2013 October 23

## SUMMARY

With seismic interferometry, reflections can be retrieved between stations positioned on the Earth's surface. In the classical form, the reflections are retrieved by a crosscorrelation of observations and an integration over subsurface sources. For a specific data set, however, the actual source distribution might not be sufficient to approximate the source integral. Yet, there might be a dense distribution of receivers allowing an integration over the receiver domain. We rewrite the source integral to an integration over receiver pairs and call it receiver-pair seismic interferometry (RPSI). With this formulation, reflections can be retrieved even in the limiting case of only a single source. We illustrate the new relation both with synthetic data and data from the USArray, which is a large grid of stations covering the USA. The field observations are from an earthquake in Mexico. We show that RPSI can be applied both for a line and grid of receivers. When using isolated phases recorded over a line of stations inline with the earthquake, reflections are retrieved from the core-mantle boundary, which reflections can be ascribed to specific virtual source and receiver locations within the USArray. When using full responses as input to RPSI, the retrieved phases are an average over multiple virtual sources and receivers. Location is then only possible when the integrand is spatially windowed or when a clear leading term is identified. When using a grid of receivers, the location of the source does not need to be known, but spatially averaged instead of localized responses are obtained, also when isolated arrivals are used as input to RPSI.

**Key words:** Interferometry; Composition of the mantle; Body waves; North America.

## 1 INTRODUCTION

Over the past decade scientists have developed new ways to use the crosscorrelation of wavefields as a preprocessing step for imaging. With seismic interferometry (SI), new responses are generated by crosscorrelating seismic observations and stacking over sources (e.g. Larose *et al.* 2006; Snieder *et al.* 2009; Wapenaar *et al.* 2010). When SI is applied to two stations, the waves are filtered out that traveled between the two station positions. Thus, after applying SI, the response is obtained as if one of the stations acts as a virtual source to the other. The location and character of the actual sources does not need to be known, as long as they provide a rich distribution of wavefields that is recorded at both stations. After applying SI, the virtual source location is known. Moreover, complex wavefields, for example coda from earthquakes or noise-source observations, are turned into simpler wavefields. For these reasons, the responses retrieved with SI are more amenable for Earth imaging than the

originally recorded wavefields. Consequently, SI makes it possible to obtain higher resolution images without changing the sensor configuration.

When SI is applied to body waves, reflections can be retrieved between station positions. In the classical form (e.g. Wapenaar & Fokkema 2006) the reflections are retrieved by crosscorrelating observations and integrating the crosscorrelation results over subsurface sources, Huygens' sources (e.g. Derode *et al.* 2003), or normal modes (Lobkis & Weaver 2001). This processing does not provide new data. However, it enables extraction of conceivable responses from complicated observations. With the goal of retrieving reflections, the correlation integral has been applied for many configurations with sufficient sources to integrate over (e.g. van Manen *et al.* 2005; Bakulin & Calvert 2006; Draganov *et al.* 2007; Miyazawa *et al.* 2008; Zhan *et al.* 2010; Nakata *et al.* 2011; Ruigrok *et al.* 2011; van der Neut *et al.* 2011; Carrière & Gerstoft 2013). For specific configurations, however, the actual source distribution is not sufficient to approximate the source integral, nor is there enough scattering or a sufficiently diffuse wavefield. A pragmatic solution has been the application of an additional stacking over the receiver domain. Draganov *et al.* (2009) applied a so-called brute stack after

\* Now at: Department of Earth Sciences, Utrecht University, PO Box 80.021, 3508 TA Utrecht, the Netherlands.

applying SI, to yield the signal-to-noise (S/N) of exploration-scale reflections. Also Poli *et al.* (2012), Nishida (2013), Lin *et al.* (2013) and Boué *et al.* (2013) applied additional stacking over the receiver domain to obtain reflections from the mantle transition zone and core-mantle boundary (CMB). When using multiple sources and applying an additional stacking over receivers, lateral resolution over the receiver domain is lost; averaging takes place over multiple reflection points.

In this paper we show that, for specific settings, it is possible to retrieve reflections using only one source, without averaging over multiple reflection points. We take advantage of the availability of a well-sampled receiver array and write an interferometric relation that employs an integration over receiver pairs instead of over sources. We call this method receiver-pair seismic interferometry (RPSI). By studying the integrand of the interferometric relation, the retrieved phases can be localized to virtual source and receiver positions within the array.

The method is scale independent and can be applied to dimensions ranging from laboratory setups to global-scale seismology. In the following, we first discuss the underlying correlation integral for isolated phases. Next, we illustrate the method using a regional scale numerical example and consider the use of full wavefields. Subsequently, we apply RPSI to USArray data (Levander *et al.* 1999) to retrieve reflections from the CMB.

## 2 ISOLATED-PHASE RPSI

In this section, we introduce RPSI using isolated phases. The use of isolated phases allows a simple stationary-phase derivation of the interferometric relation (Appendix). Furthermore, it gives the basis for an expansion to full wavefields (Section 3). In Section 2.1, we explain the method and in Section 2.2 we illustrate the method using a regional-scale numerical example.

### 2.1 Methodology

We introduce RPSI using the 2-D configuration as depicted on Fig. 1. Assume we have one large array of receivers. The receivers are located on a flat free surface and thus their location is given with only a horizontal coordinate. The first receiver is located at  $x_{\min}$  and the last receiver at  $x_{\max}$ . We consider a subsurface source at  $\mathbf{x}_S$ , whose wavefield contains reflected travel paths within the array. The precise location of the source is not relevant. Further, we define

midpoint  $m$  as a location between two receivers and the half-offset  $h$  as the distance from  $m$  along the array to one of the two receivers. If the medium of consideration is approximately 1-D and  $m - h \geq x_{\min}$  and  $m + h \leq x_{\max}$  for a range of  $m$ , we can evaluate the following interferometric relation

$$\int_{\partial\mathbb{S}_0} X(m-h, \mathbf{x}_S, -t) * XY(m+h, \mathbf{x}_S, t) dm \propto -Y(m_o+h, m_o-h, t), \quad (1)$$

where the asterisk  $*$  denotes a temporal convolution and a proportionality sign is used since we have left out the amplitude terms.  $X(m-h, \mathbf{x}_S, t)$  denotes an arrival observed at location  $m-h$  (one of the receivers in the array) due to a source at  $\mathbf{x}_S$  and  $XY$  is an arrival that includes  $X$  and one or more additional free-surface reflected travel paths. The retrieved phase (the one on the right-hand side in eq. 1) is  $Y(m_o+h, m_o-h, t)$ , which is an (reflection) arrival as if there were a source and receiver at the free surface, at locations  $m_o-h$  and  $m_o+h$ , respectively.  $\partial\mathbb{S}_0$  is the line segment of midpoints over which is integrated and  $m_o$  is the stationary midpoint (Fig. 1).

In Fig. 1, relation 1 is illustrated for a half-offset equal to 2.5 receiver spacings, and seismic phases  $X$  and  $XY$  corresponding to a direct wave and a (primary) ghost reflection, respectively. Ray paths with the same colour denote the direct wave and ghost reflection that are recorded by the first and second receiver in a receiver pair. These are the arrivals that are crosscorrelated, yielding a so-called correlation event. Through integration, the stationary-phase zone of correlation events stacks in constructively, whereas other amplitudes interfere destructively (Snieder 2004, and Appendix). When we denote the integrand of eq. (1) with  $I$ ,  $m_o$  is the stationary point, that is the location where  $dI/dm = 0$ . Hence,  $m_o$  can directly be estimated from the integrand. The largest arrival-time difference for ray paths with the same colour is occurring when the direct wave and the first leg of the ghost reflection overlap, which happens for the cyan rays. The crosscorrelation of these cyan rays gives the stationary contribution to the integral ( $m = m_o$ ). By stacking the crosscorrelations,  $-Y(m_o+h, m_o-h, t)$  is retrieved, which corresponds here to a primary reflection. This phase is depicted at the right-hand side in Fig. 1. Note that  $m_o-h$  and  $m_o+h$  are within the array of receivers, but do not necessarily collocate with actual receiver positions.

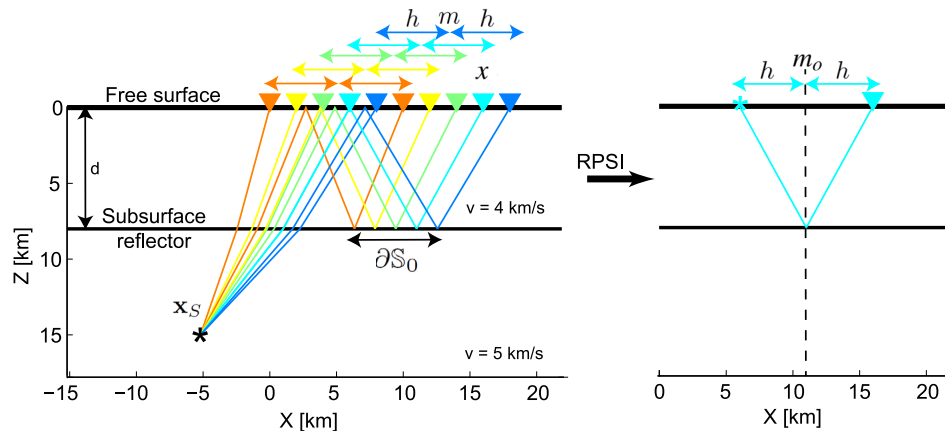


**Figure 1.** (Left) A body-wave configuration for receiver-pair seismic interferometry (RPSI). The response of a subsurface source (star at  $\mathbf{x}_S$ ) is measured with an array of receivers (coloured triangles). (Right) After applying RPSI the reflection is obtained as if there were a source at location  $m_o-h$  and a receiver at  $m_o+h$ , where  $m_o$  is the stationary midpoint for the primary reflection at half-offset  $h$ , from the interface at depth  $d$ .

In eq. (1), receiver pairs are crosscorrelated with a fixed distance of  $2h$ . For a fixed  $h$ , a receiver pair is uniquely defined by its midpoint  $m$ . Thus, the integration over midpoint is effectively an integration over receiver pairs. Hence, the name ‘receiver-pair seismic interferometry.’ RPSI differs from interferometric relations with integration over sources (e.g. Wapenaar 2004) or receivers (e.g. Hong & Menke 2006; Curtis *et al.* 2009). As with other types of SI, with RPSI a response is retrieved between two positions. These positions are located on the free surface, within the array. An additional stationary-phase analysis is required to find the positions of the virtual source:  $m_o - h$  and the virtual receiver:  $m_o + h$ . If the retrieved phase is a primary reflection or a turning wave, it has its reflection point or turning point vertically below (or close to) the stationary midpoint  $m_o$ .

Eq. (1) is derived in Appendix with a stationary-phase approximation, for one choice of  $X$  and  $XY$ . The same relation can be derived for dipping layers. In this case, the reflection point of the retrieved arrival does not lay vertically below the stationary midpoint, but is deflected updip. In media with triplications, applying the correlation integral (the left-hand side of eq. 1) leads to the retrieval of arrival  $Y$  for more than one station pair.

Eq. (1) also holds for finding reflections with midpoints in between two (similarly oriented) arrays of receivers. In this case, a range of  $m$  is chosen in between the arrays, for which  $m - h$  coincides with locations in array 1 and  $m + h$  coincides with locations in array 2.

## 2.2 Numerical illustration

We illustrate eq. (1) using a modification to the regional-scale configuration as depicted in Fig. 1. The spatial sampling of the array is densified from  $dx = 2$  km to  $dx = 0.5$  km. Furthermore, the array is extended from  $x = 18$  km to  $x = 23$  km, yielding a total of 47 stations. The layer depth  $d$  remains at 8 km and also the source remains at  $\mathbf{x}_S = (x, z) = (-5.2, 15)$  km. The velocity  $v$  of the first layer is  $4 \text{ km s}^{-1}$ .

Fig. 2(a) depicts the input data for RPSI, which is the direct wave, labelled  $X$  and the ghost reflection  $XY$  due to the subsurface source. The traces in Fig. 2 have the same colour coding as in Fig. 1. To this data we apply eq. (1) for  $h = 5$  km. Thus, first we crosscorrelate traces from stations at  $2h$  distance, yielding Fig. 2(b), which is the crosscorrelation panel. Subsequently, we stack the crosscorrelations over midpoint, yielding Fig. 2(c), in which the main pulse is the retrieved reflection  $Y$ , with its polarity flipped.

We do not isolate arrivals prior to crosscorrelation. We merely cut-off the response after the relevant ghost reflection. Hence, the crosscorrelation yields all possible cross terms (4: one due to crosscorrelation of  $XY$  with  $X$ ,  $XY$  with  $XY$ ,  $X$  with  $X$  and  $X$  with  $XY$ ). We call these cross terms correlation events. For this example, only the correlation event arising from a crosscorrelation between  $X$  and  $XY$  (the highlighted one) gives a stationary contribution. That is, amplitudes sum constructively in a zone of midpoints where the derivative with respect to midpoint becomes zero. The three other

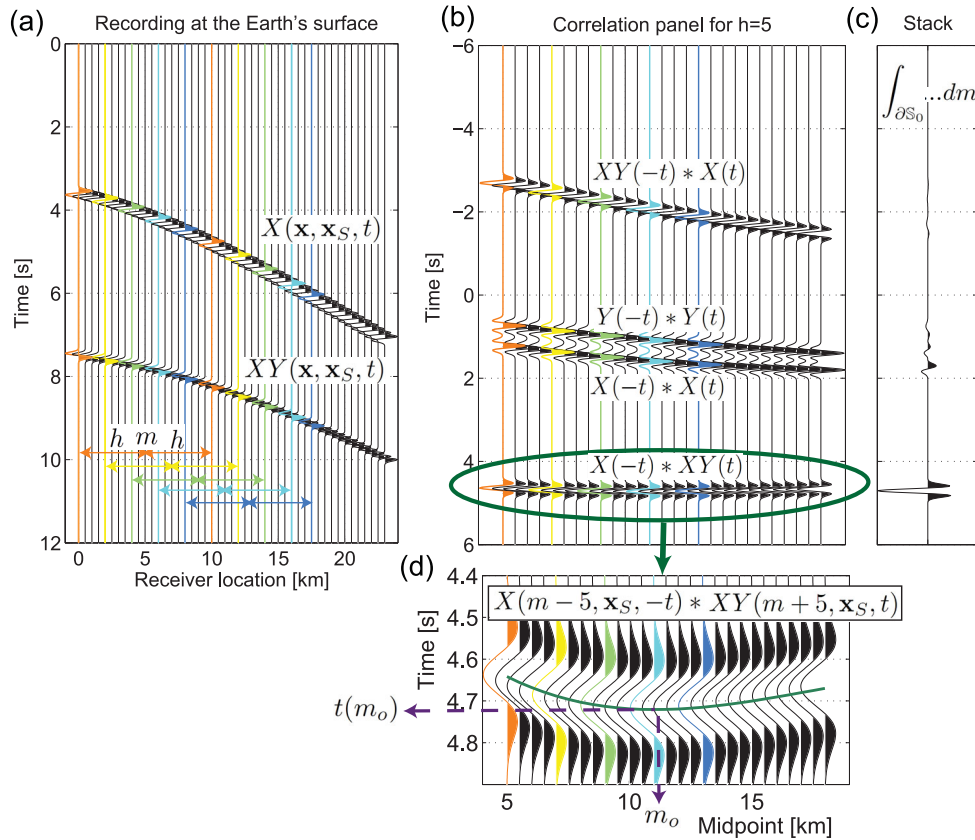


**Figure 2.** A regional-scale numeric example of receiver-pair seismic interferometry (RPSI). (a) A direct wave  $X$  and ghost reflection  $XY$  due to a subsurface source, recorded with an array of receivers. (b) The result of crosscorrelating receiver pairs in (a). All receiver pairs have the same distance  $2h$ , but varying midpoint  $m$ . Crosscorrelation of the two orange traces in (a) gives the first trace in (b). The same colour coding is used in Fig. 1. All other traces in (b) are found from crosscorrelating successive receiver pairs. (c) A stack of (b) over midpoints, which is the result of RPSI. (d) an enlargement of the crosscorrelation event in (b), which gives a stationary contribution to (c).

correlation events do not reach stationarity. Still, these events give small contributions to the stack (Fig. 2c) due to a sudden cut-off of the integration domain. These edge effects could be suppressed by applying a taper.

Fig. 2(d) shows an enlargement of the correlation event with the stationary contribution. In this panel, the stationary midpoint  $m_o$  can be picked to locate the virtual source position  $m_o - h$  and receiver position  $m_o + h$  that belong to the retrieved reflection  $Y$ . Furthermore,  $t(m_o)$  can be picked, which is the two-way traveltime of the retrieved reflection. The such estimated time, 4.72 s, is equal to the actual traveltime  $(\sqrt{(2d)^2 + (2h)^2}/v)$ . And the picked stationary midpoint,  $m_o = 11.06$  km, corresponds to the actual midpoint (Fig. 1).

Note that we pick the arrival time in the correlation panel. Cross-correlation removes the phase of the wavelet. Consequently, the timing corresponds with the maximum absolute amplitude of the stationary phase of the correlation event. Alternatively, we could pick the timing from the maximum absolute amplitude of the retrieved arrival (in Fig. 2c). The latter is less accurate. The integration over the stationary-phase zone leads to a  $\pi/4$  shift (Appendix) that needs to be taken into account to extract the correct timing. However, the stationary-phase zone might be incompletely sampled, leading to uncertainty in the actual phase shift. Picking the timing directly in the correlation panel circumvents this issue. In case of an incomplete stationary-phase zone, the difference in timing from the pick in the correlation panel and after stacking, could be used to correct the phase of the retrieved arrival.

### 3 FULL-WAVEFIELD RPSI

In the previous section, we considered RPSI applied to isolated phases (eq. 1). This application of RPSI makes it necessary to time window phases before application. In the numerical example (Section 2.2) we applied only a bottom mute, leading to three more cross terms, and showed that these cross terms stack out destructively. For, for example, noise sources it is not possible to apply this bottom mute. To allow wider applicability, in this section we evaluate RPSI for complete wavefields. With conventional SI, the use of complete responses and integration over subsurface sources yields complete responses (Wapenaar & Fokkema 2006). This is not the case for RPSI, as we will see.

We find an expression for full wavefields, by first replacing in eq. (1) the partial responses  $X$  and  $XY$  by full responses  $G$ , where  $G$  stands for the impulse response or Green's function. The output of full-wavefield RPSI can be written as a sum of the outputs of isolated-phase RPSI. We need to take the following into account.

(i) The full response contains ghost reflections from multiple layers. Hence, the output of full wavefield RPSI contains a sum of arrivals. These arrivals include primary reflections from the different interfaces and higher order arrivals.

(ii) Due to the limited extent of the receiver array, the retrieved sum of arrivals might not be equal to the complete response; some of the stationary-phase zones might not be captured by the midpoint integration.

(iii) For each retrieved arrival, the stationary midpoint, and hence the virtual source and receiver, may be at a different position. We illustrate this point in Fig. 3.

(iv) Correlation events with different stationary midpoints may give contributions to the same retrieval. We illustrate this point in Fig. 3.

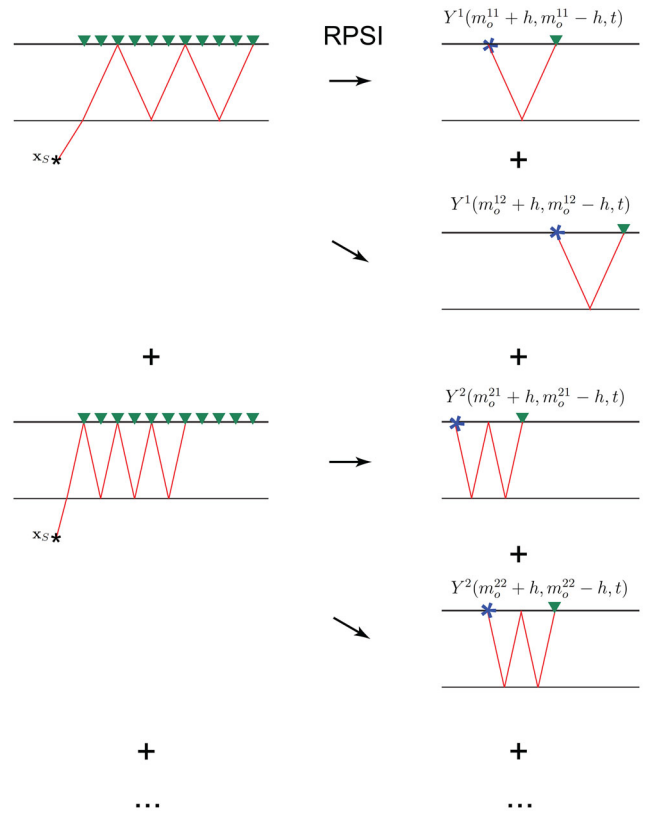


**Figure 3.** (Left) a ray visualization (red lines) of arrivals that are part of the input for full-wavefield RPSI (eq. 2) and (right) a ray visualization of the corresponding output. The drawings are made for a layer-over-a-half-space model (two horizontal lines) with a real source in the half-space (star) and receivers on the free surface (triangles). The four retrieved phases, as drawn on the right-hand side, all have the same half-offset  $h$ , but varying midpoint locations  $m_o^{ij}$ , where  $i$  is a phase-index and  $j$  is a stationary-midpoint index.

(v) Cross terms which are not due to  $X$  with  $XY$  stack out destructively (Fig. 2). The exception is for input phases with a linear moveout (refractions and surface waves). In this case, the crosscorrelation of  $X$  with  $X$  (with  $X$  being a linear phase) remains stationary for a range of midpoints.

Thus, accounting the above points, the relation for full-wavefield RPSI reads

$$\int_{\partial\mathbb{S}_0} G(m-h, \mathbf{x}_S, -t) * G(m+h, \mathbf{x}_S, t) dm \propto \sum_{i=1}^n \sum_{j=1}^{p^i} -Y^i(m_o^{ij} + h, m_o^{ij} - h, t), \quad (2)$$

where  $Y^i$  denotes a retrieved phase,  $i$  is a seismic-phase index and  $j$  is a stationary-midpoint index. The output of eq. (2) is a collection of phases. Hence, the sum over  $n$  phases. For retrieving phase  $Y^i$  there might be multiple stationary contributions over the array. Hence, the summation over  $p^i$  contributions.

Fig. 3 shows (left) stationary arrivals within an array of stations that (right) lead to retrieval of different phases, and at different stationary midpoints, but all at the same offset. Only a subset of all possible stationary contributions is shown. When full wavefields are used, the result of RPSI is thus the sum of, among others, all the phases depicted on the right-hand side of Fig. 3. Note that for each retrieval there is a leading contribution. For example  $Y^1(m_o^{11} + h, m_o^{11} - h, t)$  has a much higher amplitude than



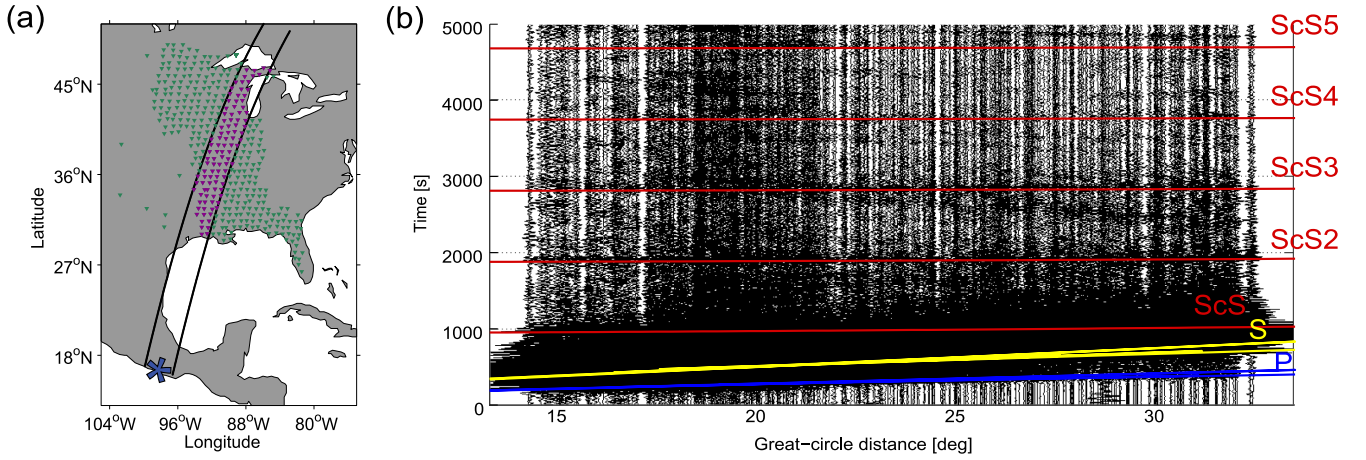


**Figure 4.** (a) Map view of a part of the USArray stations (triangles) and the location of an earthquake in Mexico (star). All stations are used for 3-D RPSI (Section 5), while only the purple subset is used for 2-D RPSI (Section 4). (b) The east-west recording earthquake response after bandpass filtering and whitening. Indicated with red lines are the timing of the primary shear-wave core-mantle boundary reflection  $ScS$  and its multiples  $ScSi$ , where  $i$  is an order index. The timings were found by raytracing through an 1-D Earth model (Knapmeyer 2004).

$Y^1(m_o^{12} + h, m_o^{12} - h, t)$ ; for a reflection coefficient  $r = 0.1$  the first contribution to  $Y^1$  has a  $r/r^3 = 100$  times larger amplitude than the second contribution. Thus,  $Y^1$  may be approximated to have only a single stationary midpoint at  $m_o^{11}$ . This approximation allows location of the retrieved phase. Alternatively, the contributions from multiple stationary midpoints can be separated in the correlation panel, to obtain localized estimations of  $Y^i$  rather than averages over multiple stationary midpoints.

#### 4 FIELD DATA

Since 2006, seismic stations from the USArray transportable array (e.g. Burdick *et al.* 2012) have covered a large part of the contiguous USA. At each moment in time, a grid of sensors is simultaneously recording, which makes it ideal data for applying RPSI. The continental scale of the array makes a spherical-stratified model a better approximation than a horizontally layered model, as was used for illustrating RPSI in the previous sections. Yet, also for a spherical Earth, eqs (1) and (2) remain valid.

We use recordings of the  $M_w = 7.4$  Oaxaca (Mexico) earthquake, which occurred 2012 March 20, on a depth of 20 km. Fig. 4(a) shows a distribution of USArray stations that recorded the earthquake. We apply RPSI to a linear subarray. Hence, from the grid of stations we select a band of receivers that is inline with the earthquake source. In Section 4.1, we apply isolated phase RPSI (Section 2) to retrieve one reflection at a single offset. In Section 4.2, we apply full-wavefield RPSI (Section 3) successively to retrieve multiple reflections for a large offset range.

##### 4.1 Single offset

We apply RPSI for the configuration as depicted on Fig. 5. Thus, in eq. (1) we substitute  $X$  and  $XY$  by shear-wave core-reflected phases  $ScS2$  and  $ScS3$ , respectively. Applying RPSI would in this case yield  $Y = ScS$  within the USArray. As preprocessing, we take the data from the purple stations in Fig. 4(a), apply bandpass filtering between 0.01 and 0.04 Hz and interpolate the data to a regular station spacing. Next, we time-window  $ScS2$  and  $ScS3$  and apply eq. (1) for  $h = 4^\circ$ , yielding Fig. 6(a). The left-hand panel shows the result after crosscorrelation, at times around the correlation event with

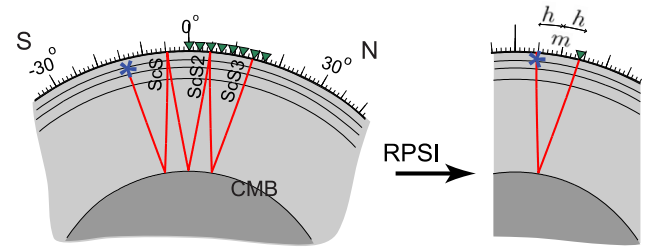


**Figure 5.** Left: a section view of  $ScS$ ,  $ScS2$  and  $ScS3$  due to the earthquake in Mexico. The latter two phases are shown being recorded with a line of stations (green triangles) from the USArray (Fig. 4). Right: the result of applying receiver-pair seismic interferometry (RPSI).  $ScS$ , an  $S$ -wave reflection from the core-mantle boundary (CMB), is retrieved within the array of stations.

a stationary phase. The right-hand graph depicts the retrieved  $ScS$  phase with flipped polarity (due to the minus sign on the right-hand side of eq. 1). Note that there is very little moveout of the correlation event (i.e.  $dt/dm$  is small). Hence, we enlarge the time axis in order to determine the stationary midpoint  $m_o$ , yielding Fig. 6(b). In this panel, the maximum values are picked for each midpoint position. The resulting time-midpoint function (the kinematics of the correlation event) is fitted with a degree 4 polynomial, giving the red line in Fig. 6(b). This polynomial is used to find an accurate pick of the stationary midpoint:  $m_o = 8.64^\circ$  and the two-way traveltime of the retrieved phase:  $t(h = 4^\circ, m_o) = 938.63$  s. As a last step,  $m_o$  is used to determine the virtual source ( $m_o - h$ ) and receiver ( $m_o + h$ ) position for the retrieved  $ScS$  phase. Fig. 6(c) shows these locations.

In this procedure, the timing of  $ScS$  is obtained from the correlation panel (Fig. 6b). The timing of the retrieved reflection (right-hand side of Fig. 6a) is likely not perfect due to an incomplete stationary-phase region and interference with edge effects.

The two-way traveltime found by raytracing through the iaspei91 model (Kennett & Engdahl 1991) is 941.31 s and is a few seconds later than the timing of the retrieved event (938.63 s). This traveltime difference can be largely ascribed to the cratonic setting of the virtual source and receiver (Fig. 6c). Evaluating the upper 200 km of a recent SV-wave model [DNA13-SV joint model as described in Porritt *et al.* (2013)] we find a two-way traveltime anomaly of  $-2.57$  s below  $m_o$ .

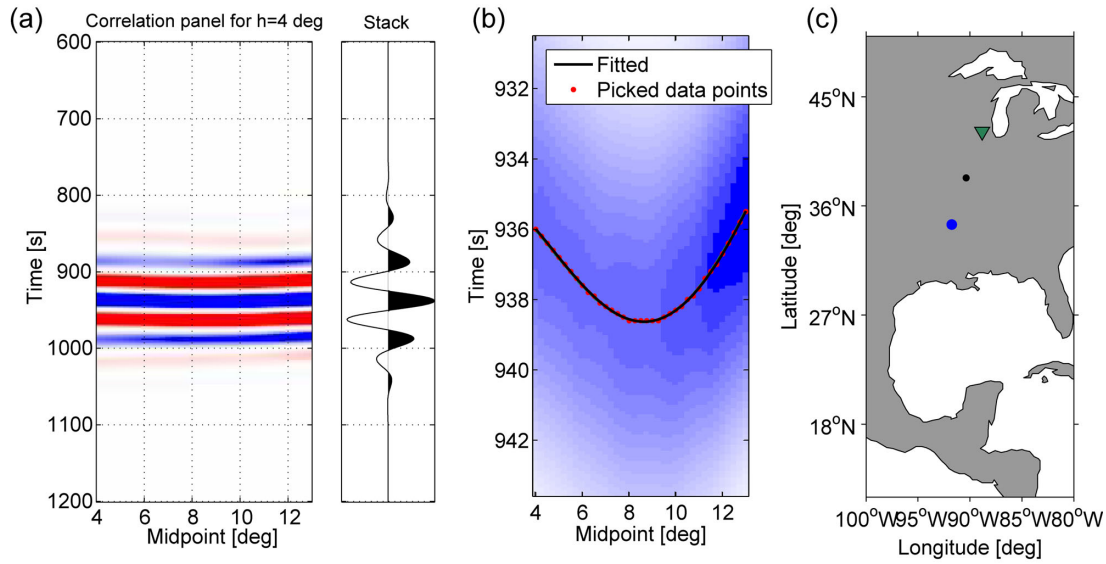


**Figure 6.** The results of applying RPSI to isolated *ScS* reverberations from the earthquake response in Fig. 4. (a) The correlation panel on the left and the retrieved *ScS* reflection (with a flipped polarity) for  $h = 4^\circ$  on the right. (b) An enlargement of the correlation event in (a), showing where stationarity is reached. (c) A map view of the stationary midpoint (the black dot) and the corresponding virtual source (blue circle) and receiver (green triangle) position for the retrieved reflection in (a).

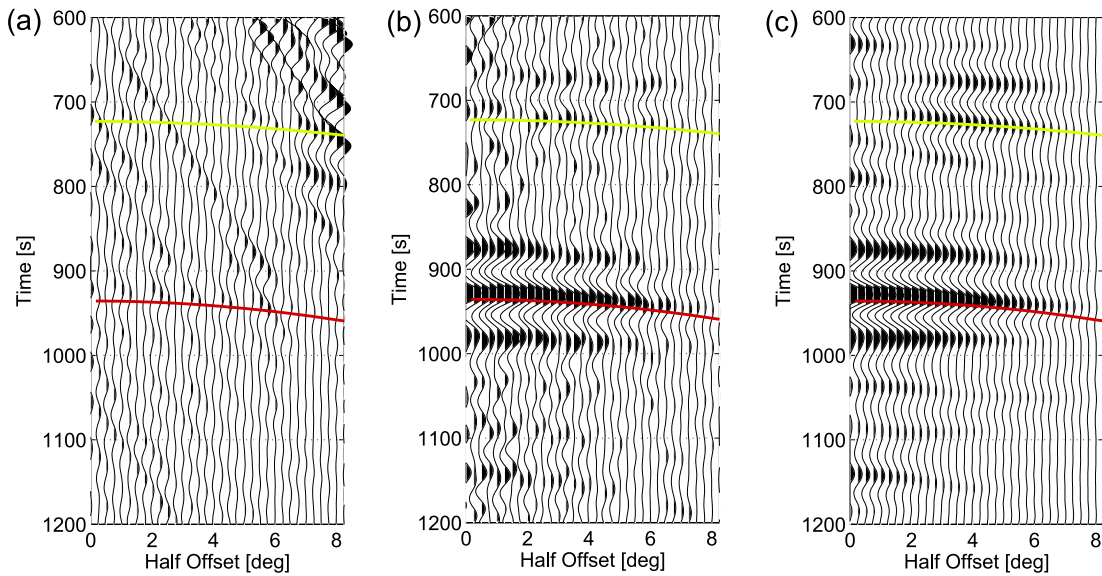


**Figure 7.** A comparison of full-wavefield RPSI (eq. 2) results for a range of offsets for the purple stations in Fig. 4(a). The *iaspei91* arrival times of *PcS* and *ScS* are denoted with a yellow and red line, respectively. Different preprocessing prior to RPSI is compared: (a) only frequency bandpass filtering, (b) additionally time-domain normalization, (c) additionally wavenumber bandpass filtering.

#### 4.2 Multioffset

Using the approach as described in the previous section, we can find *ScS* for approximately the following offset range:  $3^\circ < h < 5.5^\circ$ . We can extend the offset range by not only using contributions from crosscorrelations of *ScS2*&*ScS3*, but by also using *ScS3*&*ScS4* and *ScS4*&*ScS5* (Fig. 4b). If we were to time-window sections around higher order *ScS* reverberations we would be able to localize the stationary midpoints as we did in the previous section. Instead, in this section we only aim to extract the average *ScS* reflection response of the subsurface below the purple triangles in Fig. 4a. We use the full recordings until 5000 s after the earthquake and accept that retrievals of *ScS* might be an average over multiple stationary contributions, as illustrated in Fig. 3.

To the regularized data, we apply eq. (2) successively for  $h$  ranging from  $0^\circ$  to  $8^\circ$ , with steps of  $0.25^\circ$ . Fig. 7 compares three different preprocessing approaches. In Fig. 7(a) only bandpass filtering is applied to the data prior to crosscorrelation. In this case, the recordings remain dominated by surface waves and thus mainly surface waves are retrieved. In the time window around the expected arrival time of *ScS*, denoted with the red line, only surface-wave remnants can be distinguished. In Fig. 7(b) running-absolute-mean normalization (Bensen *et al.* 2007) is applied in the time domain, to equalize the amplitudes of the recordings over the duration of the traces. Each sample in a trace is divided by the mean of absolute values of the surrounding samples in a window of 125 s duration. This has a marked effect on the RPSI result: the surface-wave

remnants largely disappear whereas *ScS* appears above the noise level. Still the (S/N) is limited. This is, amongst others, caused by the fact that the correlation panels are not sufficiently sampled in space for all occurring correlation events. Crosscorrelations of arrivals with large moveout differences lead to correlation events with large moveout. Due to spatial aliasing, not all amplitudes outside the stationary-phase zones interfere destructively. Besides, the edges of the integration give rise to spurious contributions. Fig. 7(c) shows the RPSI result after wavenumber filtering and running-absolute-mean normalization. With the filtering, the larger wavenumbers are removed from the input data. Consequently, all arrivals with large moveout, like surface waves, are suppressed. The RPSI result shows a much cleaner *ScS* retrieval than without wavenumber filtering. The moveout largely follows the red line, which is the raytraced arrival time for *iaspei91* (Dziewonski & Anderson 1981; Kennett & Engdahl 1991). As before, *ScS* is slightly faster than *iaspei91* due to the cratonic setting of the array (Fig. 4a). After wavenumber filtering, not only *ScS* is retrieved more cleanly, but also *PcS* (denoted with the yellow line) is retrieved for the larger offsets. Note the long effective zero-phase source-time functions overlying the reflections, due to the narrow-band of low frequencies ([0.01 0.04] Hz). Besides *PcS* and *ScS* there are no other prominent phases in the plotted time window ([600 1200] s). Hence, the remaining amplitudes in Fig. 7(c) are either more complicated arrivals, or remaining edge effects.

### 5 3-D FULL-WAVEFIELD RPSI

In this section, we consider a grid of stations as depicted on Fig. 4(a). This grid consists of 418 receivers ( $n = 418$ ) and  $n(n-1)/2 = 87153$  receiver pairs. We define  $h$  as an absolute horizontal offset. Unlike in Section 4, there are many station pairs that are not inline with the source. To uniquely describe a station pair, besides midpoint and offset, we add the receiver-pair azimuth  $\theta$ . For a grid of stations, when we apply the crosscorrelation for one offset, like in eq. (2), and stack the crosscorrelations, implicitly we sum both over midpoint and azimuth. In Ruigrok & Wapenaar (2013) it is shown that the integration over azimuth becomes stationary for the station-pairs that are inline with the source. Hence, the following intuitive relation can be written

$$\oint_{\theta=0}^{2\pi} \int_{S_0} G(\mathbf{x}_A, \mathbf{x}_S, -t) * G(\mathbf{x}_B, \mathbf{x}_S, t) d^2 \mathbf{m} d\theta \\ \propto \sum_{i=1}^n \sum_{j=1}^{p^i} \left\{ -Y^i(\mathbf{x}_{VR}^{ij}, \mathbf{x}_{VS}^{ij}, t) + Y^i(\mathbf{x}_{VR}^{ij}, \mathbf{x}_{VS}^{ij}, -t) \right\}, \quad (3)$$

where

$$\mathbf{x}_A = (x, y) = (m_x - h \sin \theta, m_y - h \cos \theta), \quad (4)$$

$$\mathbf{x}_B = (m_x + h \sin \theta, m_y + h \cos \theta), \quad (5)$$

$$\mathbf{x}_{VR}^{ij} = (m_{xo}^{ij} + h \sin \theta_S, m_{yo}^{ij} + h \cos \theta_S) \quad \text{and} \quad (6)$$

$$\mathbf{x}_{VS}^{ij} = (m_{xo}^{ij} - h \sin \theta_S, m_{yo}^{ij} - h \cos \theta_S). \quad (7)$$

In the above equations,  $\mathbf{x}_A$  and  $\mathbf{x}_B$  denote the first and second receiver position in a receiver pair, respectively.  $\mathbf{m}_o = (m_{xo}, m_{yo})$  and  $\theta_S$  are a stationary midpoint and a stationary azimuth, respectively.  $\mathbf{x}_{VR}$  and  $\mathbf{x}_{VS}$  are the virtual receiver and source position, respectively.  $S_0$  spans a surface distribution of midpoints and  $\theta$  is integrated over a all possible azimuths.

In eq. (3) there are, in comparison with eq. (2), two additional integrations: one over the second midpoint coordinate and one over receiver-pair azimuth  $\theta$ . The integrand becomes stationary for  $\theta$  at, or close to, the backazimuth of the source  $\theta_S$ . As in the 2-D case (Section 3) multiple phases are retrieved (hence the sum over  $n$ ) and for each phase multiple stationary midpoints exist (hence the sum over  $p^i$ ). In the 3-D case there is a larger amount of stationary midpoints  $p^i$  than in the 2-D case, as we will see in the following. In summary, evaluating the integral on the left-hand side of eq. (3) for half-offset  $h$  yields a collection of phases  $Y^i$  for which stationarity is achieved at different stationary midpoints  $\mathbf{m}_o^{ij}$  below the array, for receiver pairs with azimuths equal, or close to,  $\theta_S$ .

Due to integrating the azimuth over  $2\pi$ , for each receiver pair, the one trace is crosscorrelated with the other, but also in reversed order. Consequently, a collection of phases  $Y^i$  is not only retrieved at positive times, but also at negative times. Hence, the additional time-reversed arrivals at the right-hand side of eq. (3).

Prior to applying eq. (3) to the field data (Fig. 4a), we apply running-absolute-mean normalization (as in Section 4) to the recorded data. Subsequently, we crosscorrelate the data at all station pairs and group the crosscorrelations in half-offset bins with a size of  $0.25^\circ$ . Thus, the first bin contains crosscorrelations of station pairs with half-offsets ranging from  $0^\circ$  to  $0.25^\circ$ . Next, we stack the crosscorrelations in each bin, yielding Fig. 8(a). Fig. 8(b) shows the result of 2-D RPSI as discussed in Section 4. Comparing Figs 8(a) and (b) one sees that the same events are retrieved. However, the S/N is higher for the 3-D implementation, especially at the larger offsets.

Fig. 8(c) shows the result when using records with a duration of 20 000 s after the earthquake as input to 3-D RPSI, rather than only the first 5000 s, as in Figs 8(a) and (b). Comparing Figs 8(a) and (c) one sees that *ScS* and *ScS2* are retrieved with a more confined wavelet when 20 000 s are used (Fig. 8c). Thus, it turns out that high-order reverberations ( $> \text{ScS5}$ , which occur at times larger than 5000 s after the earthquake) still contribute to the retrieval. In Fig. 8(c), at the near offset, the S/N drops somewhat, probably caused by coherent, non-earthquake related, energy at later times.

For obtaining Fig. 8 we used the East (E) component for all station pairs. As can be seen on Fig. 9, E is close to the transverse component for the stationary station pairs. In general, though, the source location will be unknown and better results would be obtained when taking the transverse component defined with respect to the station-pair azimuths.

Fig. 9 shows an approximation of the 3-D RPSI stationary contributions for retrieving *ScS* for the offset bin  $3.5^\circ < h < 3.75^\circ$ . Figs 9(a) and (b) show the stationary receiver-pair paths and midpoints, respectively. Both for 2-D and 3-D RPSI there are contributions from crosscorrelations of different phases (both from the combination *ScS2*&*ScS3* and *ScS3*&*ScS4* in this case). However, for the 3-D implementation there are lateral spreads of stationary midpoints, whereas for the 2-D implementation there is only a single stationary midpoint for each phase combination. The higher S/N with 3-D RPSI thus stems from averaging over a larger spread of stationary midpoints.

### 6 DISCUSSION

We evaluated three different implementations of RPSI:

(i) Isolated phase RPSI (Sections 2 and 4.1, eq. 1). The advantage of this approach is that the retrieved phases can be localized and accurate timing is possible. A disadvantage is that it involves



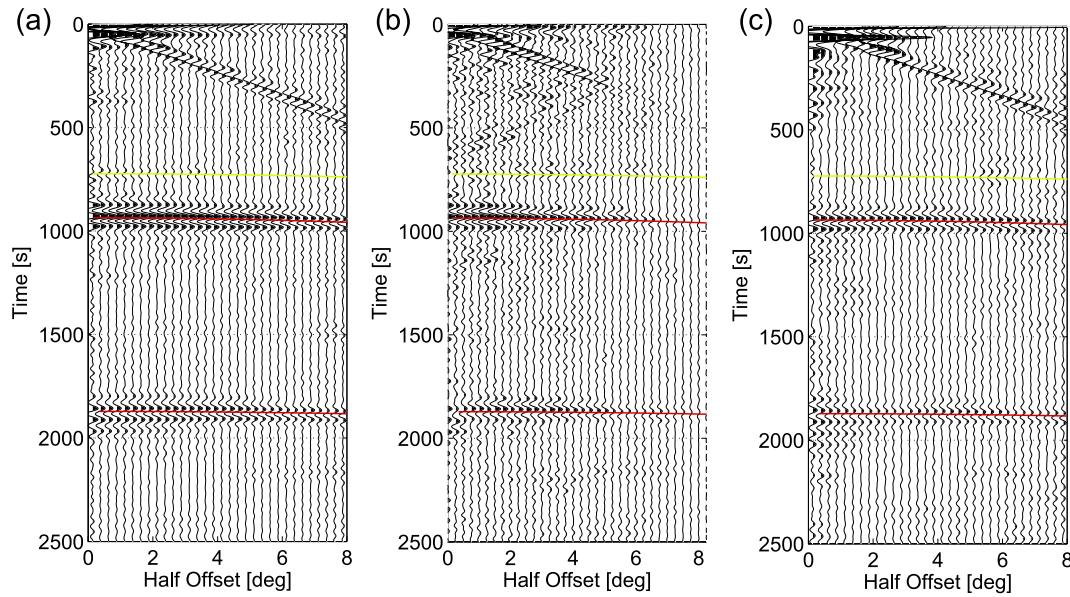


**Figure 8.** A comparison of multioffset responses retrieved with (a) 3-D RPSI and (b) 2-D RPSI, using the same preprocessing to the input data. (b) is a copy of 7(b), but it is shown for a longer duration. The yellow and red lines denote the iaspei91 arrival times of  $PcS$  and  $ScS$ & $ScS2$ , respectively. (c) 3-D RPSI using 20 000 s input data instead of 5000 s.

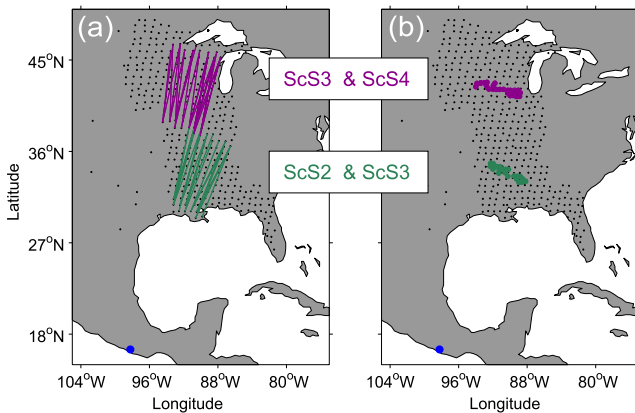


**Figure 9.** (a) Lines connecting station pairs and (b) corresponding mid-points that give stationary contributions to the integral in eq. (3) (3-D RPSI) for retrieving  $ScS$  at half-offset:  $3.5^\circ < h < 3.75^\circ$ , using the response at the receivers (black dots) of one large earthquake (blue dot). Both the crosscorrelation of  $ScS2$ & $ScS3$  (green lines/points) and the crosscorrelation of  $ScS3$ & $ScS4$  (purple lines/points) give stationary contributions. For the computation of the stationary points it is assumed that the earthquake (blue dot) is at zero km depth and that the Earth is radially symmetric.

additional processing (time windowing phases) which can only be applied for transient sources with known approximate locations.

(ii) 2-D full-wavefield RPSI (Section 3 and 4.2, eq. 2). The advantage of this approach is that no time windowing is required and hence the method can also be applied for noise sources. A disadvantage is that, as with the previous method, this technique is to be applied to a line of receivers approximately inline with the source (hence the source location needs to be approximately known). When no effort is done to separate different contributions in the correlation panel, an average of responses over the array is obtained. This is clearly undesirable for delineating structure that shows large variation over the array.

(iii) 3-D full wavefield RPSI (Section 5, eq. 3). The advantage of this approach is that the location of the source does not need to be

known. However, the structure is averaged over the array. As with the 2-D implementation, different contributions could be separated in the correlation panel to yield localized retrievals, but this will be a tedious exercise when using a grid of receivers.

In the previous sections, RPSI was applied for a single source. The availability of multiple sources allows a successive application of RPSI to retrieve phases at multiple offsets for the same midpoint (with eq. 1). With a straightforward implementation of full-wavefield RPSI (eqs 2 and 3) averaged responses over the array were obtained (e.g. Fig. 8). The (S/N) of these averaged responses is improved by stacking in retrievals obtained with different sources. The averaged responses remain localized below the array, irrespective of the earthquake locations and depths. When sufficient sources are available to apply conventional SI, responses can be retrieved that are again localized to specific virtual-source and receiver positions.

In Section 4.1, a procedure was applied to obtain an accurate timing of a retrieved reflection,  $ScS$  in this case. This procedure could be repeated for multiple offsets and multiple earthquakes in order to get accurate timing of  $ScS$  or other phases over the USArray. After taking into account heterogeneous structure in the crust and mantle, the timings can be used for delineating the CMB topography below the USA.

The timings of phases found with RPSI are not affected by source uncertainties. As with conventional seismic interferometry, the exact location of the source is not relevant and source-timing errors similarly affect different stations and are subtracted in the interferometric process. Non-synchronous recording over the array is an issue and timing mismatches between different stations need to be corrected before applying RPSI.

The stationary-phase zone of RPSI expresses the zone of receiver-pair combinations that contribute in phase to a retrieval. For a reflection, the size of the stationary-phase zone is indicative of the size of the sensitivity kernel at the reflection surface. In Fig. 6(a), it was shown that the stationary-phase zones for retrieving  $ScS$  are extensive; at the edges of the correlation panel, the time difference of



the correlation event with respect to the stationary-phase point were still less than one-fourth a period. Hence, the sensitivity kernels for  $ScS$  are extensive for the low frequencies for which it could be retrieved. This challenges the ability to image the CMB topography with high spatial resolution.

With respect to using directly measured  $ScS$ ,  $ScS$  retrieved with RPSI has a slightly lower frequency content, due to attenuation of the higher order reverberations that were used for retrieving the phase. On the bright side, with RPSI  $ScS$  can be retrieved between many station positions within the array and uncover information that was previously hidden in the coda of a response.

Traditional array methods are commonly used to boost the (S/N) of core phases (Rost & Thomas 2002). When one source is used, amplitudes from the same phase are added up over array elements and noise is suppressed to the cost of lateral resolution (by stacking time-shifted data over offset and azimuth). With RPSI, phases are retrieved from the intrinsic relation between different orders of reverberations, without sacrificing resolution (by stacking crosscorrelated data over midpoint). If desired, also to the result of RPSI, traditional array methods can be applied to boost the (S/N) of the retrieved phases.

For global-scale SI, a dense sampling of sources is required to retrieve complete responses between station positions (Ruigrok *et al.* 2008). This dense sampling only exists locally. 3-D RPSI explains why still nearly complete average responses could be obtained (Boué *et al.* 2013; Lin *et al.* 2013; Nishida 2013). In these three references, grids of receivers were used and crosscorrelations between all possible receivers pairs were grouped in offset bins and stacked over the bins. This operation can be described as a successive implementation of eq. (3) for a range of offsets. As input data, recordings of multiple years were utilized. Crosscorrelating long traces with multiple source responses is equivalent to crosscorrelating isolated source responses and stacking over sources [i.e. conventional SI (Wapenaar & Fokkema 2006)]. Hence, the high S/N ratio achieved can be ascribed to averaging over multiple stationary midpoints in the receiver-pair domain (3-D RPSI) and additionally stacking over stationary sources in the source domain (conventional SI). By doing so, Lin *et al.* (2013) obtained high-quality global phases averaged over regional arrays and Nishida (2013) and Boué *et al.* (2013) averaged over the entire globe.

## 7 CONCLUSIONS

We introduced RPSI, which is a method to retrieve phases within an array of sensors. Unlike other interferometric relations, only observations of a single source are used as input. The method consists of the following steps. First, the observations are grouped in pairs of receivers with the same offset  $2h$ , or within the same offset bin. Secondly, the two observations in each receiver pair are crosscorrelated. Thirdly, the crosscorrelation results in each offset bin are stacked. The above steps yield an estimation of arrivals that are both induced and recorded within the array of sensors, with an offset  $2h$  between the virtual source and receiver position. When isolated phases are used as an input for RPSI, it is possible to localize a retrieved phase. That is, the virtual source and receiver position can be found by determining at which midpoint position the integrand becomes stationary. When full responses are used as an input, the retrieved arrivals are an average over multiple virtual sources and receivers. Unique location is then only possible when the correlation panel is spatially windowed in different contributions, or when a clear leading term is identified.

We illustrated RPSI both with synthetic and field data. The field observations were from an earthquake in Mexico, observed by US-Array stations. We showed that RPSI can be applied both with a line and a grid of receivers. When using isolated phases recorded over a line of stations inline with the earthquake, reflections were retrieved from the CMB, which could be ascribed to specific virtual source and receiver locations within the USA. When using full wavefields recorded over a line or grid of receivers, multiple stationary contributions existed. Consequently, average responses over the array were obtained.

## ACKNOWLEDGEMENTS

This research is supported by the The Netherlands Research Centre for Integrated Solid Earth Sciences (ISES). I would like to thank Kees Wapenaar, Joachim Ritter and an anonymous reviewer for numerous suggestions that helped improve this work. Data from the TA network were made freely available as part of the Earth-Scope USArray facility, operated by Incorporated Research Institutions for Seismology (IRIS) and supported by the National Science Foundation, under Cooperative Agreements EAR-0323309, EAR-0323311, EAR-0733069.

## REFERENCES

- Bakulin, A. & Calvert, R., 2006. The virtual source method: theory and case study, *Geophysics*, **71**(4), SI139–SI150.
- Bensen, G., Ritzwoller, M., Barmin, M., Levshin, A., Lin, F., Moschetti, M., Shapiro, N. & Yang, Y., 2007. Processing seismic ambient noise data to obtain reliable broad-band surface wave dispersion measurements, *Geophys. J. Int.*, **169**, 1239–1260.
- Bleistein, N., 1984. *Mathematical Methods for Wave Phenomena*, Academic Press.
- Boué, P., Poli, P., Campillo, M., Pedersen, H., Briand, X. & Roux, P., 2013. Teleseismic correlations of ambient seismic noise for deep global imaging of the Earth, *Geophys. J. Int.*, **194**, doi:10.1093/gji/ggt160.
- Burdick, S. *et al.*, 2012. Model update March 2011: upper mantle heterogeneity beneath North America from travel time tomography with global and USArray Transportable Array data, *Seism. Res. Lett.*, **83**, 23–28.
- Carrière, O. & Gerstoft, P., 2013. Deep-water subsurface imaging using OBS interferometry, *Geophysics*, **78**(2), Q15–Q24.
- Curtis, A., Nicolson, H., Halliday, D., Trampert, J. & Baptie, B., 2009. Virtual seismometers in the subsurface of the earth from seismic interferometry, *Nat. Geosci.*, **2**, 700–704.
- Derode, A., Larose, E., Campillo, M. & Fink, M., 2003. How to estimate the Green's function of a heterogeneous medium between two passive sensors? Application to acoustic waves, *Appl. Phys. Lett.*, **83**, 3054–3056.
- Draganov, D., Wapenaar, K., Mulder, W., Singer, J. & Verdel, A., 2007. Retrieval of reflections from seismic background-noise measurements, *Geophys. Res. Lett.*, **34**, L04305, doi:10.1029/2006GL028735.
- Draganov, D., Campman, X., Thorbecke, J., Verdel, A. & Wapenaar, K., 2009. Reflection images from ambient seismic noise, *Geophysics*, **74**(5), A63–A67.
- Dziewonski, M. & Anderson, D.L., 1981. Preliminary reference earth model, *Phys. Earth planet. Inter.*, **25**, 297–356.
- Hong, T.-K. & Menke, W., 2006. Tomographic investigation of the wear along the San Jacinto fault, southern California, *Phys. Earth planet. Inter.*, **155**, 236–248.
- Kennett, B. & Engdahl, E., 1991. Traveltimes for global earthquake location and phase identification, *Geophys. J. Int.*, **105**, 429–465.
- Knapmeyer, M., 2004. TTBox: a Matlab toolbox for the computation of 1D teleseismic travel times, *Seism. Res. Lett.*, **75**, 726–733.
- Larose, E. *et al.*, 2006. Correlation of random wavefields: theory and application, *Geophysics*, **71**(4), SI11–SI21.

- Levander, A., Humphreys, E., Ekstrom, G., Meltzer, A. & Shearer, P., 1999. Proposed project would give unprecedented look under North America, *EOS, Trans. Am. geophys. Un.*, **80**, 245–251.
- Lin, F.-C., Tsai, V., Schmandt, B., Duputel, Z. & Zhan, Z., 2013. Extracting seismic core phases with array interferometry, *Geophys. Res. Lett.*, **40**, 1049–1053.
- Lobkis, O. & Weaver, R., 2001. On the emergence of the Green's function in the correlations of a diffuse field, *J. acoust. Soc. Am.*, **110**, 3011–3017.
- Miyazawa, M., Snieder, R. & Venkataraman, A., 2008. Application of seismic interferometry to extract P- and S-wave propagation and observation of shear-wave splitting from noise data at Cold Lake, Alberta, Canada, *Geophysics*, **73**, doi:10.1190/1.2937172.
- Nakata, N., Snieder, R., Tsuji, T., Lerner, K. & Matsuoka, T., 2011. Shear wave imaging from traffic noise using seismic interferometry by cross-coherence, *Geophysics*, **76**(6), SA97–SA106.
- Nishida, K., 2013. Global propagation of body waves revealed by cross-correlation analysis of seismic hum, *Geophys. Res. Lett.*, **40**, 1–6.
- Poli, P., Campillo, M. & Pedersen, H., 2012. Body-wave imaging of Earth's mantle discontinuities from ambient seismic noise, *Science*, **338**, 1063–1065.
- Porritt, R.W., Allen, R.M. & Pollitz, F.F., 2013. Seismic imaging east of the Rocky Mountains with USArray, *Earth planet. Sci. Lett.*, doi:10.1016/j.epsl.2013.10.034.
- Rost, S. & Thomas, C., 2002. Array seismology: methods and applications, *Reviews of Geophysics*, **40**, 1008, doi:10.1029/2000RG000100.
- Ruigrok, E. & Wapenaar, K., 2013. Receiver-pair seismic interferometry and the cosine method, in *Proceedings of 75th EAGE Conference & Exhibition incorporating SPE EUROPEC*, extended abstracts, Th 15 11.
- Ruigrok, E., Draganov, D. & Wapenaar, K., 2008. Global-scale seismic interferometry: theory and numerical examples, *Geophys. Prospect.*, **56**, 395–417.
- Ruigrok, E., Campman, X. & Wapenaar, K., 2011. Extraction of P-wave reflections from microseisms, *Comptes Rendus Geosci.*, **343**, 512–525.
- Snieder, R., 2004. Extracting the Green's function from the correlation of coda waves: a derivation based on stationary phase, *Phys. Rev. E*, **69**, 046 610-1–046 610-8.
- Snieder, R., Miyazawa, M., Slob, E., Vasconcelos, I. & Wapenaar, K., 2009. A comparison of strategies for seismic interferometry, *Surv. Geophys.*, **30**, 503–523.
- van der Neut, J., Thorbecke, J., Mehta, K., Slob, E. & Wapenaar, K., 2011. Controlled-source interferometric redatuming by crosscorrelation and multidimensional deconvolution in elastic media, *Geophysics*, **76**(4), SA63–SA76.
- van Manen, D., Robertsson, J. & Curtis, A., 2005. Modeling of wave propagation in inhomogeneous media, *Phys. Rev. Lett.*, **94**, 164 301-1–164 301-4.
- Wapenaar, K., 2004. Retrieving the elastodynamic Green's function of an arbitrary inhomogeneous medium by cross-correlation, *Phys. Rev. Lett.*, **93**, 254 301-1–254 301-4.
- Wapenaar, K. & Fokkema, J., 2006. Green's functions representations for seismic interferometry, *Geophysics*, **71**(4), SI33–SI46.
- Wapenaar, K. & Thorbecke, J., 2013. On the retrieval of the directional scattering matrix from directional noise, *SIAM J. Imaging Sci.*, **6**, 322–340.
- Wapenaar, K., Draganov, D., Snieder, R., Campman, X. & Verdel, A., 2010. Tutorial on seismic interferometry: Part 1-Basic principles and applications, *Geophysics*, **75**(5), 75A195–75A209.
- Zhan, Z., Ni, S., Helmberger, D. & Clayton, R., 2010. Retrieval of Moho-reflected shear wave arrivals from ambient seismic noise, *Geophys. J. Int.*, **182**, 408–420.

## APPENDIX A: STATIONARY-PHASE ANALYSIS

In this appendix, we derive eq. (1) with a stationary-phase approximation for a configuration akin to Fig. 1. We consider 2-D wave propagation in the vertical plane due to a source at  $\mathbf{x}_S = (0, z_S)$ .

For sake of simplicity, we assume here that there is only a density contrast between an upper layer and a half-space below and we treat the layer and half-space as lossless homogeneous fluids. For phases  $X$ ,  $XY$  and  $Y$  in eq. (1), we choose a direct wave (denoted with  $u^{dw}$ ), a ghost reflection ( $u^{gh}$ ) and a primary reflection ( $u^{r1}$ ), respectively. In the frequency domain, the direct-wave far-field ( $kr \gg 1$ ) monopole response at receiver location  $\mathbf{x} = (x, z) = (m - h, 0)$  can be written as

$$u^{dw}(m - h, \mathbf{x}_S, \omega) = \frac{1}{\sqrt{8\pi k r^{dw}}} e^{-j(kr^{dw} + \frac{\pi}{4})}, \quad (\text{A1})$$

where  $j$  is the imaginary unit,  $k = \omega/v$ ,  $k$  is the wavenumber,  $\omega$  is the angular frequency,  $v$  is the propagation velocity and a horizontal position is given as function of a midpoint  $m$  and half-offset  $h$ .  $r^{dw}$  is the distance traversed by the direct wave:  $r^{dw} = \sqrt{(m - h)^2 + (z_S)^2}$ . Similarly, the ghost-reflection response recorded at  $\mathbf{x} = (m + h, 0)$  can be expressed as

$$u^{gh}(m + h, \mathbf{x}_S, \omega) = \frac{R_{10}R_{12}}{\sqrt{8\pi k r^{gh}}} e^{-j(kr^{gh} + \frac{\pi}{4})}, \quad (\text{A2})$$

where  $r^{gh}$  is the distance traversed by the ghost reflection:  $r^{gh} = \sqrt{(m + h)^2 + (z_S + 2d)^2}$ , with  $d$  denoting the depth of the interface.  $R_{10}$  and  $R_{12}$  are the reflection coefficients between layer 1 and the free surface, and layer 1 and the half-space, respectively. Cross-correlating eqs (A1) and (A2) and integrating over a line distribution of midpoints  $m$  yields

$$\begin{aligned} & \int_{\partial\mathbb{S}_0} \{u^{dw}(m - h, \mathbf{x}_S, \omega)\}^* u^{gh}(m + h, \mathbf{x}_S, \omega) dm \\ &= \int_{\partial\mathbb{S}_0} \frac{R_{10}R_{12}}{8\pi k \sqrt{r^{dw}r^{gh}}} e^{-jk(r^{gh} - r^{dw})} dm, \end{aligned} \quad (\text{A3})$$

where  $\partial\mathbb{S}_0$  denotes the domain spanned by the midpoint distribution and  $*$  denotes complex conjugation.

We split up the phase term in eq. (A3),  $-k(r^{gh} - r^{dw})$ , into  $k$  and a phase function:

$$\begin{aligned} \phi(m) &= -(r^{gh} - r^{dw}) = -\sqrt{(m + h)^2 + (z_S + 2d)^2} \\ &\quad -\sqrt{(m - h)^2 + (z_S)^2}. \end{aligned} \quad (\text{A4})$$

Moreover, we define the amplitude function:

$$A(m) = \frac{|R_{10}|R_{12}}{8\pi k \sqrt{r^{dw}(m)r^{gh}(m)}}. \quad (\text{A5})$$

With these substitutions, eq. (A3) can be written as

$$\int_{\partial\mathbb{S}_0} -A(m) e^{jk\phi(m)} dm. \quad (\text{A6})$$

The phase in the integrand of eq. (A6) is stationary when  $d\phi/dm = \phi'(m) = 0$ . We compute the phase-function derivative with respect to  $m$ :

$$\phi'(m) = \frac{-m - h}{\sqrt{(m + h)^2 + (z_S + 2d)^2}} + \frac{m - h}{\sqrt{(m - h)^2 + (z_S)^2}} \quad (\text{A7})$$

and the second derivative:

$$\begin{aligned} \phi''(m) &= \frac{-1}{\sqrt{(m + h)^2 + (z_S + 2d)^2}} + \frac{(m + h)^2}{((m + h)^2 + (z_S + 2d)^2)^{3/2}} \\ &\quad - \frac{1}{\sqrt{(m - h)^2 + (z_S)^2}} + \frac{(m - h)^2}{((m - h)^2 + (z_S)^2)^{3/2}}. \end{aligned} \quad (\text{A8})$$

and solve eq. (A7) for  $\phi'(m) = 0$  to find the stationary point:

$$m_o = \frac{h(d + z_s)}{d}. \quad (\text{A9})$$

For large  $|kr|$  eq. (A3) can be approximated as (Bleistein 1984; Wapenaar & Thorbecke 2013)

$$-\sqrt{\frac{2\pi}{k|\phi''(m_o)|}} A(m_o) e^{j(k\phi(m_o) + \mu \frac{\pi}{4})} \propto -e^{j(k\phi(m_o) + \mu \frac{\pi}{4})}, \quad (\text{A10})$$

where  $\mu = \text{sign}(k\phi''(m_o))$ . On the right-hand side of eq. (A10) we left out the amplitude terms, but we kept in the polarity reversal due to the underside free-surface reflection ( $R_{10}$ ). By substituting eq. (A9) into (A4) we calculate the value of the phase function at the stationary point:

$$\phi(m_o) = -\sqrt{\left(\frac{h(2d + z_s)}{d}\right)^2 + (z_s + 2d)^2} - \sqrt{\left(\frac{hz_s}{d}\right)^2 + (z_s)^2}. \quad (\text{A11})$$

The upper expression can be simplified to

$$\phi(m_o) = -\sqrt{(2d)^2 + (2h)^2}. \quad (\text{A12})$$

Furthermore, by substituting eq. (A9) into eq. (A8) we find that  $\text{sign}(\phi''(m_o)) = -1$  for any choice of  $h$ ,  $d$  and  $z_s$  (which are always positive values) and hence  $\mu = \text{sign}(k\phi''(m_o)) = -1$  for positive  $k$ . Thus, by combining eq. (A3), (A10) and (A12) we find the kinematic

stationary-point approximation for the correlation integral:

$$\begin{aligned} & \int_{\partial\mathbb{S}_0} \{u^{dw}(m - h, \mathbf{x}_S, \omega)\}^* u^{gh}(m + h, \mathbf{x}_S, \omega) dm \\ & \propto -e^{-j(k\sqrt{(2d)^2 + (2h)^2} + \frac{\pi}{4})} \\ & = -e^{-j(kr^{r1} + \frac{\pi}{4})} \propto -u^{r1}(m_o + h, m_o - h, \omega), \end{aligned} \quad (\text{A13})$$

where  $r^{r1}$  is the distance traversed by the primary reflection. Thus, by applying RPSI (the left-hand side of eq. (A13)) the primary reflection is obtained as if there were a source at location  $(x, z) = (m_o - h, 0)$  and a receiver at  $(m_o + h, 0)$ . The phase is correctly retrieved. The retrieved amplitude depends on the magnitude and the distance of the actual source.

Applying, to eq. (A13), an inverse Fourier transform to the time domain yields

$$\begin{aligned} & \int_{\partial\mathbb{S}_0} u^{dw}(m - h, \mathbf{x}_S, -t) * u^{gh}(m + h, \mathbf{x}_S, t) dm \\ & \propto -u^{r1}(m_o + h, m_o - h, t), \end{aligned} \quad (\text{A14})$$

where the asterisk  $*$  denotes a temporal convolution. Following the same derivation as above, eq. (A14) can be derived for different choices of arrivals. For example replacing in the correlation integral  $u^{gh}$  with a multiple ghost reflection, would yield a multiple reflection. When also  $u^{dw}$  is replaced by a primary ghost, then again a primary reflection is retrieved. Eq. (1) is the generalized form for isolated-phase RPSI.